Rank M-Type Radial Basis Function (RMRBF) Neural Network for Pap Smear Microscopic Image Classification

Francisco J. Gallegos-Funes,
Margarita E. Gómez-Mayorga,
José Luis Lopez-Bonilla,
Rene Cruz-Santiago.
National Polytechnic Institute of Mexico,
Mechanical and Electrical Engineering Higher School,
Av. IPN s/n, U.P.A.L.M. SEPI-ESIME, Edif. Z, Acceso 3,
3er. Piso, Col. Lindavista, 07738, Mexico, D.F., Mexico.
email: fgallegosf@ipn.mx

In this paper we present the capability of the Rank M-Type Radial Basis Function (RMRBF) neural network in the classification of Pap smear microscopic images. From simulation results we observe that the RMRBF neural network has better classification capabilities in comparison with other RBF based algorithms.

Keywords: Rank M-type Radial Basis Function neural network, Pap smear microscopic images.

1. Introduction

The cervical cancer is the second most common cancer in women worldwide and the leading cause of cancer mortality for women in developing countries [1-3]. A Papanicolaou test or Pap smear is a medical screening method that can help prevent cervical cancer. The main purpose of the Pap smear is to detect cell abnormalities that may occur in cervical cancer or before cancer develops. The automatic analysis of Pap smear microscopic images is one of the most interesting fields in biomedical image processing [4-9].

Recently, we proposed the Rank M-Type Radial Basis Function (RMRBF) Neural Network for artificial data classification and mammographic image analysis [10,11]. The RMRBF neural network uses the Median M-Type (MM) estimator [12] in the scheme of radial basis function to estimate the parameters of proposed neural network according with the schemes found in the references [13,14].

In this paper, the Rank M-Type Radial Basis Function (RMRBF) Neural Network is used for automatic Pap test screening process. The rest of this paper is organized as follows. Section 2 presents the proposed RMRBF neural network. Experimental results of classification capabilities for Pap smear images by using our method and other RBF based networks are presented in section 3. Finally, we draw our conclusions in section 4.

2. Rank M-Type Radial Basis Function Neural Network

The Radial Basis Function (RBF) neural networks are function approximation models that can be trained by examples to implement a desired input–output mapping [15,16]. In fact, radial basis function models are closely related to function approximation models used to

perform interpolation. Under certain mild conditions on the radial basis functions, the RBF neural networks are capable of approximating arbitrarily well any function. The performance of a radial basis function neural network depends on the number and centers of the radial basis functions, their shapes, and the method used for learning the input–output mapping. In the RBF neural network, each input is assigned to a vector entry and the outputs correspond either to a set of functions to be modeled by the network or to several associated classes [5,17,18]. The structure of the RBF neural network is depicted in Figure 1.
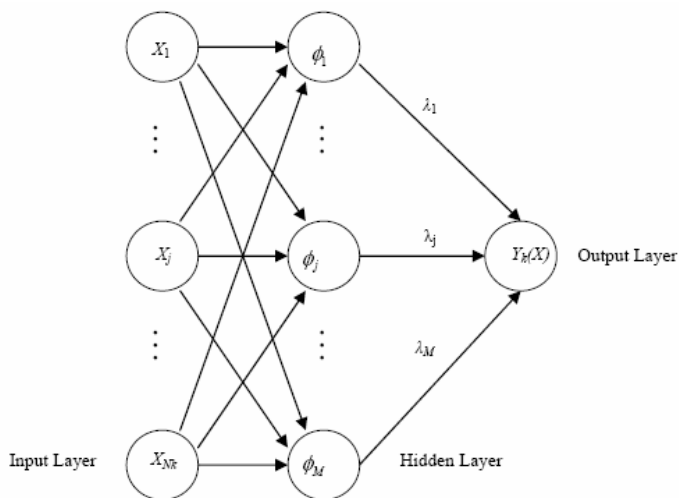

Figure 1. Structure of Radial Basis Function Neural Network.

From Figure 1, each of N_k components of the input vector X feeds forward to M basis functions whose outputs are linearly combined

with weights $\left\{\lambda_j\right\}_{j=1}^{M}$ into the network output Y_k(X). The output layer implements a weighted sum of hidden-unit outputs [13,14],

$$Y_k\left(\mathbf{X}\right) = \sum_{j=1}^{L} \lambda_{jk} \varphi_j\left(\mathbf{X}\right) \tag{1}$$

where L is the number of hidden units, M is the number of outputs with $k=1,...,M,$ the weights λ_{kj} show the distribution of the hidden unit j for modeling the output $k,$ and $\varphi_j\left(\mathbf{X}\right)$ is the activation function.

We tested with different activation functions and we chose the Gaussian function [15,16] due to this function provided the best results in the proposed application,

$$\varphi_j\left(\mathbf{X}\right) = \exp\left(-\frac{\left\|\mathbf{X} - \mu_j\right\|^2}{2\sigma_j^2}\right) \tag{2}$$

where $\mathbf{X}$ is the input vector with elements $x_i,$ μ_j is the vector determining the centre of basis function φ_j and σ is the standard deviation.

The input feature vector $\mathbf{X}$ is classified in k different clusters. The clustering k-means algorithm can be used to estimate the parameters of the RBF neural networks [15,16]. A new vector $\mathbf{x}$ is assigned to the cluster k whose centroid μ_k is the closest one to the vector. The centroid vector is updated according to,

$$\mu_k = \mu_k + \frac{1}{N_k}\left(\mathbf{x} - \mu_k\right) \tag{3}$$

where N_k is the number of vectors already assigned to the k-cluster.

In the proposed Rank M-Type Radial Basis Fuction (RMRBF) neural network we propose to use the Median M-Type (MM) estimator as robust statistics estimate of a cluster center. The MM estimator is given by [10-12],

$$\mu_k = \text{med}\left\{\mathbf{X}\tilde{\psi}\left(\mathbf{X}-\theta\right)\right\} \tag{4}$$

where $\mathbf{X}$ is the input data sample, $\tilde{\psi}$ is the normalized influence function ψ: $\psi(\mathbf{X}) = \mathbf{X}\tilde{\psi}(\mathbf{X})$, $\theta = \text{med}\{X_k\}$ is the initial estimate, $k=1, 2,\ldots,N_k$ and $\psi(X)$ is the simple cut (skipped mean) influence function given by [12],

$$\psi_{\text{cut}(r)}(X) = X \cdot 1_{[-r,r]}(X) = \begin{cases} X, & |X| \le r \\ 0, & \text{otherwise} \end{cases} \tag{5}$$

where X is a data sample and r is a real constant that depends of the data to process.

3. Experimental Results

The classification process of Pap Smear microscopic images is shown in Figure 2.
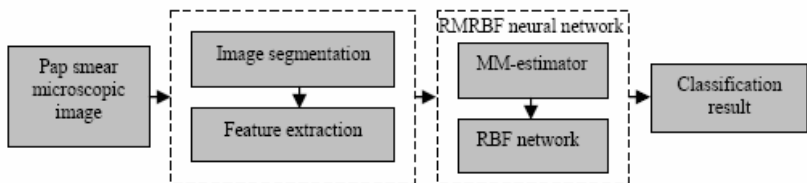

Figure 2. Block diagram of Pap Smear microscopic images classification process by using the MMRBF neural network.

In the image acquisition process, the cervical cell microscopic images were obtained from the Pathologic Anatomy Department of 1° of October Regional Metropolitan Hospital in Mexico City by means of use of Leica DME microscopy with integrated Leica EC3 digital camera, software LAS EZ (PC), and lens Leica ∞/0.17 Hi Plan 100x/1.25 oil, the size of cell images is 2048x1536 pixels [19].

The specimens, which are taken from several areas of the cervix, most often contain cells from columnar epithelium and the squamous epithelium. The squamous epithelium consists of 4 layers of cells: basal, parabasal, intermediate, and superficial cells. The Cervical intra-epithelial neoplasia (CIN), also known as dysplasia has the potential to become invasive cervical cancer. CIN is graded into three stages of severity, from CIN 1 (mild dysplasia) through CIN 2 (moderate dysplasia) to CIN 3 (severe dysplasia) [1-3,6]. Figure 3 depicts some cervical cells.

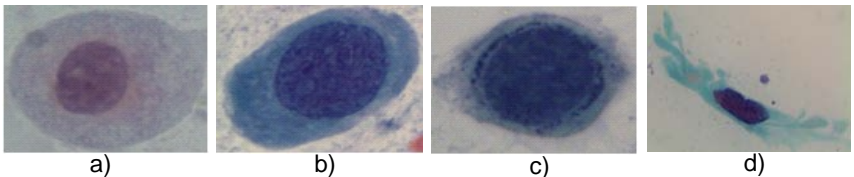
a)   b)   c)   d)

Figure 3. Basal cells, a) normal cell, b) moderate dysplasia (CIN 2), c) severe dysplasia (CIN 3) and, d) CIS (carcinoma-in-situ).

Having the Pap smear microscopic image, we proceed to segment it in 2 main regions of interest: the nucleus and cytoplasm [6,7].

The morphological image analysis can be used to perform: object extraction, image filtering operations, such as removal of small objects or noise from an image, image segmentation

operations, such as separating connected objects, and measurement operations, such as texture analysis and shape description [20,21].

The dilation and erosion are two fundamental morphological operations. Dilation adds pixels to the boundaries of objects in an image, while erosion removes pixels on object boundaries. The number of pixels added or removed from the objects in an image A depends on the size and shape of the structuring element B used to process the image. The dilation and erosion are defined as $A \oplus B$ and $A \ominus B$, respectively.

The dilation and erosion are often used in combination to implement image processing operations. A morphological opening of an image is an erosion followed by a dilation, and the morphological closing of an image, is the reverse: it consists of dilation followed by an erosion. The morphological opening and closing of an image are defined as $A \circ B = (A \ominus B) \oplus B$ and $A \bullet B = (A \oplus B) \ominus B$, respectively.

Figure 4 presents the image segmentation of a cervical cell where is displayed the cytoplasm and nucleus segmented from the original cell image.
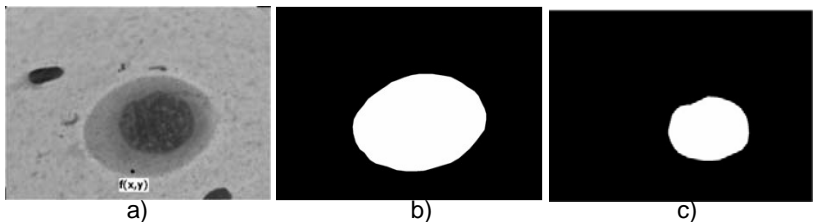

Figure 4. Image segmentation of a cervical cell, a) original cell, b) cytoplasm, c) nucleus.

We obtained 9 numerical data in the feature extraction stage [21]:

- Nucleus and Cytoplasm area,

$$area = \sum_{i}^{N} \sum_{j}^{M} seg(i,j) \qquad (6)$$

  where *seg(i,j)* are pixels of segmented object.
- Nucleus and Cytoplasm perimeter. The perimeter is the sum of the pixels that forms the contour of object.
- Nucleus and Cytoplasm Circularity,

$$Circularity = 4\pi \cdot area / perimeter^2 \qquad (7)$$

- Nucleus-Cytoplasm relation (NCR),

$$NCR = Cytoplasm \quad area / Nucleus \quad area \qquad (8)$$

- Maximum and Minimum Nucleus brightness. The image should be changed to gray scale to obtain the maximum and minimum gray value by means of use of its histogram.

Table 1 shows some numerical data obtained in the stage of feature extraction in terms of cytoplasm area (CA), cytoplasm circularity (CC), nucleus area (NA), nucleus circularity (NC), nucleus-cytoplasm relation (NCR), and maximum nucleus brightness (MNB) in the case of normal, CIN1, CIN2, CIN3, and CIS images.

Table 1. Experimental results obtained in the stage of feature extraction.

Cervical cell images	Numerical data					
	CA	CC	NA	NC	MNB	NCR
Normal	680029	0.7300	17795.2	0.8520	102.6	38.976
CIN1	50446	0.7866	50861.3	0.8630	90.33	10.723
CIN2	194935	0.7225	59347.6	0.8400	90.75	3.3854
CIN3	258753	0.6480	112275	0.8340	107.2	2.2290
CIS	178631	0.2487	40367.2	0.6980	77.75	4.7378

The described RMRBF neural network has been evaluated, and their performance has been compared with the Simple RBF and Median RBF neural networks [13,16,17].

To train the networks for getting the appropriate pdf's parameters 78 cervical cell images were used: 25 normal, 3 CIN 1 (mild dysplasia), 25 CIN 2 (moderate dysplasia), 20 CIN 3 (severe dysplasia), and 5 with CIS (carcinoma-in-situ) with microinvasive disease [15,16]. We do not consider the classification of squamous epithelium between the basal, parabasal, intermediate, and superficial cells. The objective of the experiment is to classify between different types of CIN.

For the implementation of neural networks, in the test stage we used 20 images, these images are different form the images used in the training stage. Table 2 presents the performance results obtained by applying different neural networks. From this Table, we observe that the proposed RMRBF neural network outperforms other RBF based neural networks in terms of efficiency for the classification of cervical cell images.

Table 2. Results obtained with different RBF algorithms in test stage.

Neural networks	Performance	Cervical cell images				
		Normal	CIN 1	CIN 2	CIN 3	CIS
Simple RBF	Efficiency	100%	95%	68%	70%	100%
	Error	0%	5%	32%	30%	0%
Median RBF	Efficiency	100%	100%	75%	72%	100%
	Error	0%	0%	25%	28%	0%
RMRBF	Efficiency	100%	100%	80%	77%	100%
	Error	0%	0%	20%	23%	0%

To evaluate the performance of the neural networks in terms of medical purposes, we computed the following two quantities [22].

Sensitivity is the probability that a medical test delivers a positive result when a group of patients with certain illness is under study [22],

$$Sn = TP / (TP + FN) \qquad (9)$$

where Sn is sensitivity, TP is the number of true positive that are correct, and FN is the number of false negatives, that is, the negative results that are not correct.

Specificity is the probability that a medical test delivers a negative result when a group of patients under study do not have certain illness [22],

$$Sp = TN / (TN + FP) \qquad (10)$$

where Sp is specificity, TN is the number of negative results that are correct and FP is the number of false positives, that is, the positive results that are not correct.

Table 3 shows the sensitivity and specificity values obtained for every one of the neural networks. It can be appreciated that the sensitivity of the proposed RMRBF outperforms the RFB-based networks used as comparative. In the case of specificity the proposed network obtain better results in comparison with RBF network and similar results in comparison with the Median RBF neural network.

Table 3. Sensitivity and specificity results for different Neural Networks.

Neural Networks	Sensitivity	Specificity
Simple RBF	70%	90%
Median RBF	78%	100%
Median M-type RBF	83%	100%

Finally, it is difficult to give a clinical definition of a false negative smear. The failure to detect CIN 3 is important whereas

the failure to detect a low grade abnormality, many of which regress spontaneously or progress slowly is less significant provided the woman remains in the screening program. However, even with CIN 3 lesions it is the degree of under calling which is significant, ie., if it is reported as CIN 2 or 1. For this reason the proposed RMRBF neural network has about 20% of error in the detection of CIN 2 or 3, but the proposed method can provide high efficiency in the classification of 3 groups: Normal, CINs, and CIS cells.

4. Conclusions

We present a Pap Smear microscopic image classification using the Rank M-Type Radial Basis Function (RMRBF) Neural Network. The MM-estimator is used in the scheme of radial basis function neural network to estimate the parameters of proposed RMRBF network. The results obtained with the use of the proposed RMRBF are better than the results obtained with the RBF algorithm used as comparative.

5. Acknowledgements

References

[1]   International Agency for Research on Cancer (IARC), http://www.iarc.fr/.

[2]   T.C. Wright, R.J. Kurman, and A. Ferenczy, *Cervical intraepithelial neoplasia, Pathology of the Female Genital Tract, A. Blaustein*, Springer, New York, (1994).

[3] R.J. Kurman, D.E. Henson, A.L. Herbst, K.L. Noller, and M.H. Schiffman, "Interim guidelines for management of abnormal cervical cytology", *J. Am. Med. Assoc.* **271** (1994) 11866–11869.

[4] Y.N. Mirabal, S.K. Chang, E. Neely-Atkinson, A. Malpica, M. Follen, and R. Richards-Kortum, "Reflectance spectroscopy for in vivo detection of cervical precancer", *Journal of Biomedical Optics* **7(4)** (2002) 587–594.

[5] K. Tumer, N. Ramanujam, J. Ghosh, and R. Richards-Kortum, "Ensembles of radial basis function networks for spectroscopic detection of cervical precancer", *IEEE Trans. Biomed. Eng.* **45** (1998) 953–961.

[6] M.E. Plissiti, A. Charchanti, O. Krikoni, and D.I. Fotiadis, "Automated segmentation of cell nuclei in PAP smear images", *Proc. IEEE International Special Topic Conference on Information Technology in Biomedicine*, Greece, (26 Oct 2006).

[7] J. Jantzen, and G. Dounias, "Analysis of Pap-Smear Image Data", *Proc. Nature-Inspired Smart Information Systems (2nd Annual Symposium), NISIS*, (2006)

[8] P. Mitra, S. Mitra, S.K. Pal, "Staging of cervical cancer with soft computing", *IEEE Trans. Biomedical Engineering* **47(7)** (2000) 934–940.

[9] D. Athiar Ramli, A. Fauzan Kadmin, M. Yusoff Mashor, N. Ashidi, and M. Isa, "Diagnosis of cervical cancer using hybrid multilayered perceptron (HMLP) network", *Lecture Notes in Computer Science* **3213** (2004) 591-598.

[10] J.A. Moreno-Escobar, F.J. Gallegos-Funes, V. Ponomaryov, and J.M. De-la-Rosa-Vazquez, "Radial basis function neural network based on order statistics", *Lecture Notes in Computer Science* **4827** (2007) 150-160.

[11] J.A. Moreno-Escobar, F.J. Gallegos-Funes, and V. Ponomaryov, "Median M-Type radial basis function neural network", *Lecture Notes in Computer Science* **4756** (2007) 525-533.

[12] F. Gallegos, and V. Ponomaryov, "Real-time image filtering scheme based on robust estimators in presence of impulsive noise", *Real Time Imaging* **8(2)** (2004) 78-90.

[13] A.G. Bors, and I.Pitas, "Median radial basis function neural network", *IEEE Trans. Neural Networks* **7(6)** (1996) 1351-1364.

[14] A.G. Bors, and I. Pitas, "Object classification in 3-D images using alpha-trimmed mean radial basis function network", *IEEE Trans. Image Process.* **8(12)** (1999) 1744-1756.

[15] Leica Microsystems, http://www.leica-microsystems.com/.

[16] S. Haykin, *Neural Networks, a Comprehensive Foundation*, Prentice Hall. (1994).

[17] R. Rojas, *Neural Networks: A Systematic Introduction,* Springer-Verlag. (1996).

[18] N.B. Karayiannis, and G. Weiqun Mi, "Growing radial basis neural networks: merging supervised and unsupervised learning with network growth techniques", *IEEE Trans. Neural Networks* **8(6)** (1997) 1492-1506.

[19] N.B. Karayiannis, and M.M. Randolph-Gips, "On the construction and training of reformulated radial basis function neural networks", *IEEE Trans. Neural Networks* **14(4)** (2003) 835-846.

[20] G. Ritter, *Handbook of Computer Vision Algorithms in Image Algebra*, CRC Press. (2001).

[21] H.R. Myler, and A.R. Weeks, *The Pocket Handbook of Image Processing Algorithms in C*, Prentice Hall. (1993).

[22] http://www.cmh.edu/stats/definitions/.